Macromolecules
ARTICLE

Macromolecules **2010**, *43*, 9541–9548 **9541**
DOI: 10.1021/ma1016488

Brillouin Light Scattering Investigation of the Mechanical Properties of Layer-by-Layer Assembled Cellulose Nanocrystal Films

L. Sui,[†] L. Huang,[‡] P. Podsiadlo,[§] N. A. Kotov,[†,⊥] and J. Kieffer*[,†]

[†]*Department of Materials Science and Engineering, University of Michigan, Ann Arbor, Michigan 48109, United States,* [‡]*Department of Materials Science and Engineering, Rensselaer, Troy, New York 12180, United States,* [§]*Argonne National Laboratory Center for Nanoscale Materials, Argonne, Illinois 60439, United States, and* [⊥]*Department of Chemical Engineering, University of Michigan, Ann Arbor, Michigan 48109, United States*

Received July 22, 2010; Revised Manuscript Received September 23, 2010

ABSTRACT: Composite thin films containing cellulose nanocrystal (cellN) polyanions embedded between either poly(diallyldimethylammonium chloride) (PDDA) or chitosan were fabricated using the layer-by-layer (LBL) deposition technique. The in-plane and out-of-plane elastic constants of the composites were measured using Brillouin light scattering as a function of film thickness and cellulose content. Compared to the pure cast polymer films, the addition of cellN raises the elastic constants within the growth plane by a factor of 2 and 3 for [chitosan/cellN] and [PDDA/cellN] films, respectively, while in the growth direction the elastic constant increases by 50% for [PDDA/cellN] and not at all for [chitosan/cellN]. With increasing amounts of cellN in the films, the stiffness increases in the growth plane at a higher rate than in the growth direction. These trends reflect the contribution of the cellulose nanocrystals within and cross layers to load transmission. The results are interpreted in terms of processes that occur during film deposition and the resulting spatial arrangements of the nanocrystals.

Introduction

Engineering materials derived from renewable, natural resources are becoming more important with the increase in environmental awareness; one such biomaterial is cellulose. Natural cellulose is derived predominately from plant cell walls, while animal sources from tunicate are also possible.[1−3] Its structure is composed of crystalline domains separated by amorphous regions. During hydrolysis, the amorphous regions are burnt away, leaving rod-like cellulose nanocrystals with dimensions of 5 nm in diameter and 200−400 nm in length for cotton cellulose or up to several micrometers for tunicate-derived cellulose; here they will be abbreviated as cellN.[1−4] In its nanocyrstalline form, cotton cellN has a very high stiffness. A single cellN has a reported axial Young's modulus of 100−160 GPa, depending on its degree of crystallinity,[5,6] and a transverse Young's modulus of ∼30 GPa.[6] As one of the most abundant natural fibers, cellulose is also cheap, lightweight, biodegradable, and a renewable resource,[4,7,8] thus making it a desirable candidate for composite filler. Currently, cellulose fibers have already been employed as filler in packaging and automotive applications.[4,7,9]

Podsiadlo et al. demonstrated a way to incorporate cellN into thin films using hydrolyzed cotton cellulose in combination with the layer-by-layer (LBL) fabrication method.[1] LBL assembly allows for highly controlled deposition of oppositely charged electrolytes to create alternating layered structures.[10−14] Despite the recent surge of interest in LBL assembled films, a detailed understanding of how deposition conditions affect the structural stability and mechanic properties of such films is still lacking.[10,12] In this paper, we report the mechanical properties of LBL polymer/cellN composite films, measured using Brillouin light scattering (BLS). This technique allows for the measurement of elastic constants at a microscopic level and in specific directions, therefore yielding information about the orientation of the nanocrystals within the layered structure of these materials.

*To whom correspondence should be addressed. E-mail: kieffer@umich.edu.

Experimental Section

Sample Preparation. The polymers used for LBL deposition are poly(diallyldimethylammonium chloride) (PDDA), chitosan (chit), and poly(sodium styrenesulfonate) (PSS). Solutions of 1% w/v PDDA (M_w = 200 000−400 000, ρ = 1.04 g/cm^3) and PSS (M_w = 200 000, ρ = 0.801 g/cm^3) were made by diluting a concentrated stock of 20 wt % PDDA solution and dissolving PSS powder using 18 MΩ deionized water, respectively; the solutions were stirred for 1 h or until incorporated. Solutions of 0.25% w/v chitosan (M_w = 6.3 million, ρ = 0.15−0.3 g/cm^3) were made from dissolving flakes of ≥75% deacetylated chitosan in a 3% acetic acid solution; the solutions were stirred vigorously until all the flakes dissolved and a clear, homogeneous solution was obtained. PDDA, PSS powder, chitosan flakes, and acetic acid were purchased from Sigma-Aldrich.

Whatman's No. 1 filter paper (98% cotton, ρ_{cellN} = 1.61 g/cm^3)[15] purchased from Fisher Scientific was used to make the cotton cellN solutions. 5 g of powdered filter paper was hydrolyzed using a 64% w/v sulfuric acid solution for 1 h at 45 °C (*sulfuric acid is highly exothermic when mixing with water*). The supernant was decanted from solution through centrifugation, followed by three subsequent washings and final dilution of supernant in 18 MΩ deionized water; this produces a solution of 5% w/v cellN. The solution was sonicated using a probe sonicator for 1 min on ice prior to use. A detailed account of this process is described elsewhere.[16]

[Polymer/cellN] LBL films were fabricated by hand-dipping silicon substrates into electrolyte solutions; here the polymer is either PDDA or chitosan. Prior to use, Si wafers (University Wafers) were scored, broken into 2 × 5 cm slides, and cleaned using a 3:1 H_2SO_4:H_2O_2 (piranha, *highly exothermic reaction*) solution for 1 h. The polyelectrolytes were deposited onto a Si substrate using 1 min deposition time followed by rinsing using

Published on Web 10/22/2010

Table 1. Refractive Indices, q, Phonon Wavelength, and Densities of $(\text{Polymer/cellN})_x/(\text{Polymer/PSS})_y$ LBL Composites

		$x = 0$ $y = 1$	$x = 1$ $y = 9$	$x = 1$ $y = 1$	$x = 4$ $y = 1$	$x = 1$ $y = 0$
Chit	n	1.54	1.56	1.47	1.5	1.56
	$q_\perp$ (nm^{-1})	0.036	0.037	0.035	0.035	0.037
	$\lambda_{A,\perp}$ (nm)	173	171	181	177	171
	$q_\parallel$ (nm^{-1})	0.026	0.026	0.025	0.025	0.026
	$\lambda_{A,\parallel}$ (nm)	244	241	256	251	241
	ρ (g/cm^3)	1.06 ± 0.04	1.16 ± 0.04	1.29 ± 0.02	1.30 ± 0.02	1.36 ± 0.02
	% V_f(cellN)	0	28.4 ± 1.42	66.1 ± 2.83	69.4 ± 1.8	73.8 ± 2.73
PDDA	n	1.6	1.46	1.55	1.55	1.55
	$q_\perp$ (nm^{-1})	0.038	0.034	0.037	0.037	0.037
	$\lambda_{A,\perp}$ (nm)	166	182	172	172	172
	$q_\parallel$ (nm^{-1})	0.027	0.024	0.026	0.026	0.026
	$\lambda_{A,\parallel}$ (nm)	235	258	243	243	243
	ρ (g/cm^3)	0.87 ± 0.02	1.21 ± 0.01	1.38 ± 0.02	1.40 ± 0.02	1.44 ± 0.08
	% V_f(cellN)	0	37.1 ± 0.18	68.4 ± 2.92	79.4 ± 0.77	84 ± 0.9

DI water and drying with compressed air. Multilayered films were fabricated by alternating polymer and cellN deposition, accumulating films with the thicknesses of 0.5, 1.0, 1.5, 2.0, 2.5, and 3.0 μm. Films were made using cellN solutions in two separate batches, named "set A" and "set B". Finally, samples were broken in half, and one of the halves was heat-treated at 120 °C for 24 h. For comparison, pure PDDA and chitosan films were cast and dried at 80 °C in a convection oven.

Film Growth Characterization. Films with varying amounts of cellN were fabricated by replacing layers of cellN with PSS to create film structures of $[(\text{polymer/cellN})_x/(\text{polymer/PSS})_y]$, where the polymer is either chitosan or PDDA. For example, in [chit/cellN/chit/PSS] every other layer of cellN is replaced by a layer of PSS. Five film structures were made: [polymer/PSS], $[(\text{polymer/cellN})_1/(\text{polymer/PSS})_9]$, [polymer/cellN/polymer/PSS], $[(\text{polymer/cellN})_4/(\text{polymer/PSS})_1]$, and [polymer/cellN]. The growths of these films were monitored using elliposmetry; each film has a total thickness of $\sim$1 μm. The corresponding thicknesses and refractive indices were measured using a J.A. Woollam BASE-160 spectroscopic ellipsometer and a Nanofilm Technologie GmBH ellipsometer, respectively. The densities of these films were determined from mass adsorption onto a quartz crystal using a QCM200 quartz crystal microbalance (QCM) by Stanford Research Systems. Polymer or cellN was deposited onto a 5 MHz AT-cut quartz crystal; the frequency of the crystal was recorded after rinsing and drying step of each layer deposition. The crystal was cleaned using a 5% sodium chloride solution after each use.

The densities of the LBL films are calculated using the Sauerbrey equation[17]

$$\frac{\Delta m}{A} = \frac{-\Delta F\sqrt{\rho_q \mu_q}}{2{F_0}^2} \tag{1}$$

which allows us to calculate the change in mass (Δm) per unit area (A) using the resonant frequency (F_0), change in frequency (ΔF), density ($\rho_q = 2.648$ g/cm^3), and shear modulus ($\mu_q = 2.947 \times 10^{11}$ g cm^{-1} s^{-2}) of the quartz crystal. The density of the film can then be calculated using the thickness, t, determined from ellipsometry according to

$$\rho_s = \frac{\Delta m}{A}\frac{1}{t} \tag{2}$$

A list of the density for each of the films can be seen in Table 1. The volume fraction of cellN, ϕ_{cellN}, was determined by first determining the volume of cellN, V_{cellN}, calculated using the total change in mass that can be attributed to cellN layers, Δm_{cellN}

$$V_{cellN} = \frac{\Delta m_{cellN}}{\rho_{cellN}} = \frac{\Delta F_{cellN} A\sqrt{\rho_q \mu_q}}{\rho_{cellN}{F_0}^2} \tag{3}$$

and then dividing by the total volume of the film

$$\phi_{cellN} = \frac{V_{cellN}}{At} = \frac{\Delta F_{cellN}\sqrt{\rho_q \mu_q}}{\rho_{cellN}{F_0}^2}\frac{1}{t} \tag{4}$$

where ρ_{cellN} is the density of cellulose crystals (1.61 g/cm^3).

Brillouin Light Scattering. BLS is an effective method for measuring the elastic constants of thin films and multilayered thin films.[18,19] In fact, as detailed below, this method provides some unique advantages that are particularly useful for probing the adhesion between individual layers of LBL assembled films. Light is scattered by condensed matter as a result of spatial fluctuations in the refractive index, which in a first approximation can be mapped to density fluctuations.[20] Thus, the plane wave deformations associated with acoustic phonons not only provide for scattering, but as a result of their periodicity, they also establish diffraction conditions that allow one to identify the phonon propagation direction from the scattering geometry. Furthermore, the propagation of the density waves cause inelastic scattering events that result in the frequency of the scattered light to be slightly different from that of the incident light, in a manner similar to Doppler shifts. This frequency shift in the scattered light can be directly related to the velocity of sound and consequently to the elastic properties of the material.

Note that during measurement the energy imparted by the probing laser is negligibly small. Scattering is the result of thermal phonons that exist in any material at finite temperature. The measurement is therefore noninvasive, and the specimen remains in thermodynamic equilibrium at all times. The scattered light is typically sampled from a small volume (i.e., a spot $\sim$50 μm in diameter and $\sim$1 μm thick), as defined by the collection optics, providing remarkable spatial resolution. By moving the focal point, the elastic modulus of any given specimen was measured multiple times for each sample, ensuring accuracy and repeatability. A Coherent Verdi solid-state laser with a wavelength of 532 nm was used to illuminate the samples at incident powers of less than 10 mW. The laser light was focused onto the film deposited on the polished side of the Si wafer. The scattered light was collected over a period of 20−60 min and analyzed using a Sandercock tandem 6 pass Fabry−Perot interferometer. The scattering intensity from the polymer film is significantly stronger than that from silicon. In fact, for the chosen incident powers and collection times, scattering from the silicon substrate is negligible in comparison to that from the polymer film. Consequently, the collected spectra remain devoid of any signal from silicon, and all peaks can be attributed to the polymer film.

Brillouin spectra were collected with external optics configured in 180° backscattering geometry, with an incident direction slightly inclined by a small angle α with respect to the surface normal to avoid flooding the detector with excess reflected light. A schematic of the scattering setup is shown in Figure 1.

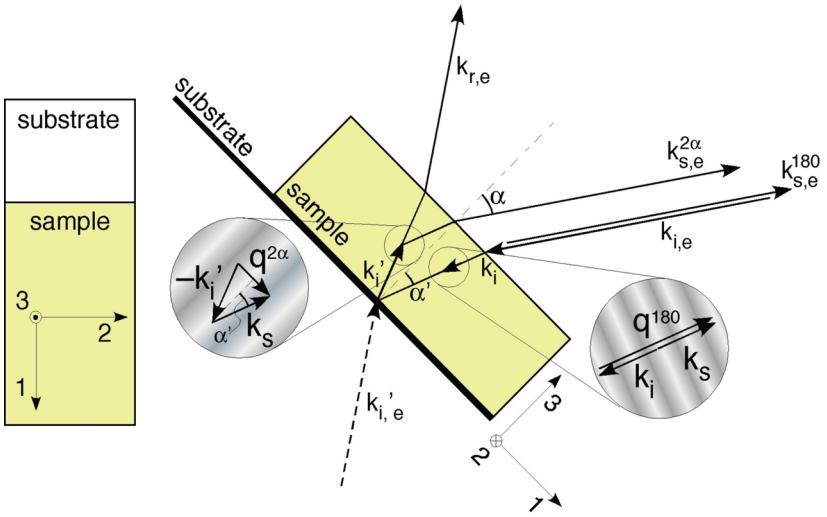

Figure 1. Brillouin light scattering in backscattering geometry. Here $\mathbf{k}_i$, $\mathbf{k}_s$, and $\mathbf{k}_r$ are the incident, scattered, and reflected beams; 1 and 2 directions are in the growth plane of the sample, and direction 3 is normal to the growth plane; α is the angle $\mathbf{k}_i$ makes with the 3 direction; $\mathbf{q}$ is the phonon whavevector, which is constructed based on the vetor sum $\mathbf{q} = \mathbf{k}_s - \mathbf{k}_i$. Accordingly, the propagation direction of the phonon probed by the direct incident beam is nearly perpendicular to that of the phonon probed by the incident beam reflected off the sample support.

The benefit of this scattering geometry is the ability to measure both the elastic constants within the plane of the film and nearly perpendicular to it, i.e., in the growth direction (or out-of-plane).[21−23] The propagation direction of the phonons probed in this measurement can be derived from the momentum balance construct shown in Figure 1. Prior to reaching the sample surface, the incident light follows the direction $\mathbf{k}_{i,e}$, which upon entering the polymer film reorients to $\mathbf{k}_i$. Light that scatters from phonons propagating in the $\pm\mathbf{q}^{180}$ direction, which is either parallel or antiparallel to $\mathbf{k}_i$, exits along the exact same path as the incident light and constitutes the backscattered radiation. For transparent materials some incident light reflects off the back surface of the film and continues along the direction $\mathbf{k}_i'$. For as long as the specimen is thin, additional scattering points (marked by the small circles) will lie within the focal volume of the collection optics. Hence, scattered light exiting the specimen along the $\mathbf{k}_{s,e}^{2\alpha}$ direction is collected at the same time as the backscattered light ($\mathbf{k}_{s,e}^{180}$). Accordingly, two peaks are observed in the Brillouin spectrum: the 180° peak and a so-called 2α peak.[23,24] To measure the elastic modulus in a particular direction of the speciment, phonons propagating in that direction must be probed using BLS, which depends on the ability to establish the appropriate scattering geometry. While the in-plane modulus in our experiments is measured in a direction perfectly parallel to the film surface, the out-of-plane modulus is measured slightly off-axis from the surface normal. Although the scattering geometry described by Cheng[18] would provide perfect alignment with the surface normal, we did not use this geometry for two reasons: (i) our films were supported on a reflective susbtrate, which would cause detector saturation by the reflected light, and (ii) many of our films were less than 2 μm thick, at which phonons may develop standing waves when aligned with the film surface normal.[18,19] Measurement of off-axis 180° phonons enables us to avoid these issues. The out-of-plane phonon wavelegth we probe is on the order of 160−180 nm, which allows for interference filtering based on 3−18 density maxima depending on film thickness, ranging from 550 to 3000 nm. In addition, with these values of wavevector magnitude, q, and film thickness, t, the product qt significantly exceeds unity, which places our measurements into the linear dispersion regime. This was verified for select samples by measuring the sound velocity as a function of the angle α, revealing equality between phase velocity and group velocity. Figure 2 shows a representative Brillouin spectrum of the anti-Stokes peaks taken in this geometry.

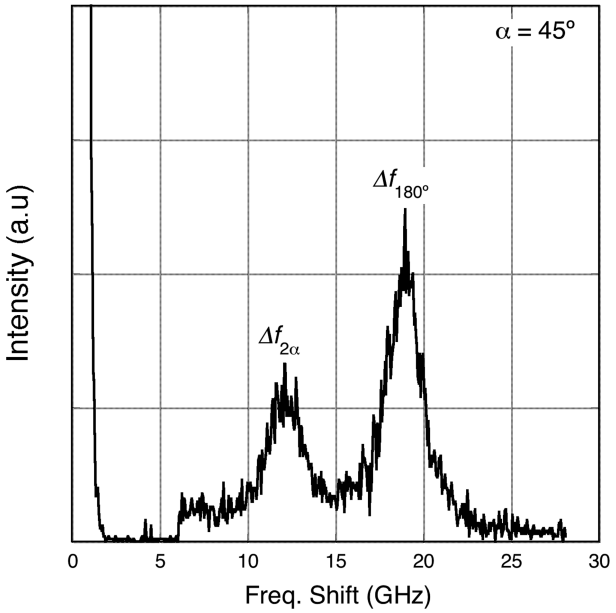

Figure 2. An exemplary Brillouin spectrum for chit/cellN on a Si wafer taken in the backscattering geometry. Peaks correspond to frequency shifts from 2α and 180° longitudinal acoustic phonons.

As can be seen from the wavevector diagram in Figure 1, the 2α peak results from light scattering from phonons propagating within the growth plane, i.e., along $\mathbf{q}^{2\alpha}$. Note that the light path giving rise to the 2α scattering is equivalent to the platelet geometry,[24] which would be achieved by replacing the reflected beam $\mathbf{k}_i'$ by one that entered the film on the substrate side following the direction indicated by $\mathbf{k}_{i,e}'$. In platelet geometry the surfaces through which the light enters and exits the sample are parallel, and the directions of the incident and scattered light form the same angle with respect to the surface normal. The sample surface, and any plane parallel to it, bisect the angle formed by $\mathbf{k}_{i,e}'$ and $\mathbf{k}_{s,e}^{2\alpha}$. Once we have identified the wavevectors of the phonons probed, we can determine their propagation velocities, according to $v = 2\pi\Delta f/q$, where Δf is the frequency shift in the Brillouin spectrum between incident and scattered light for the corresponding scattering mode. For films irradiated using a laser with a wavelength of λ, $q = (2\pi n/\lambda)\sin(\theta/2)$, where

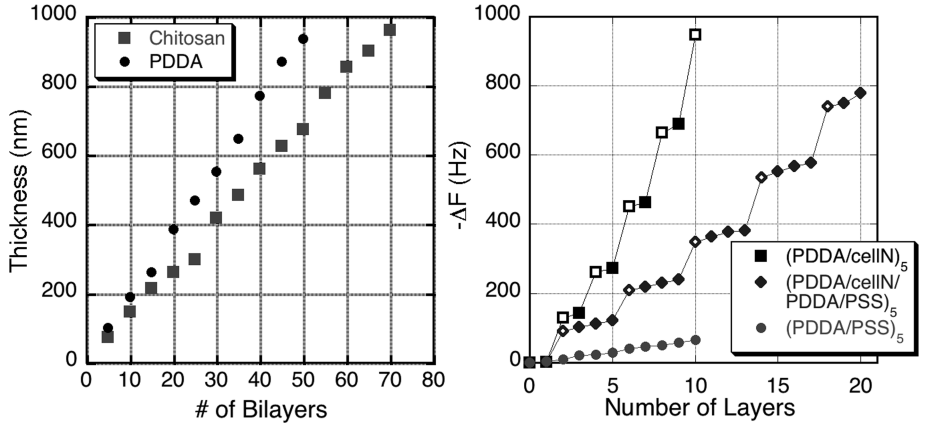

Figure 3. (A) Film thickness as a function of the number of bilayers for chitosan/cellN and PDDA/cellN layer-by-layer films. (B) Change in frequency as a function of number of layers for select PDDA/cellN films. The solid points indicate polymer growth, and open points indicate cellN growth.

n is the refractive index of the sample (Table 1). Hence, for the phonons contained within the growth plane of the sample this relationship is

$$v_{2\alpha} = \frac{\lambda \Delta f_{2\alpha}}{2n \sin \alpha'} = \frac{\lambda \Delta f_{2\alpha}}{2 \sin \alpha} \quad (5)$$

and for the backscattering mode it is

$$v_{180} = \frac{\lambda \Delta f_{180}}{2n} \quad (6)$$

In case of the 2α mode, the refractive index of the scattering medium is eliminated using Snell's law, $n \sin \alpha' = \sin \alpha$. The precise location of the peaks is obtained by fitting Lorentzian functions to the measured spectra, from which we evaluate the peak center and its full width at half-maximum. From the sound velocities and the sample density, ρ_s, and the elastic constants, $c_{\parallel,\perp}$, of the thin films can be calculated according to

$$c_{\parallel,\perp} = \rho_s v^2 \quad (7)$$

By combining eqs 1, 2, and 5−7, the longitudinal elastic constants in the growth plane ($c_\parallel$) and in the growth direction ($c_\perp$) can be determined.

Hence, using a single light scattering measurement, we can determine the elastic modulus in two different directions: in-plane and nearly perpendicular to it. The elastic modulus in growth direction is of particular interest, as it is difficult to determine by other means, and therefore provides new insights into the influence of interfaces between deposited layers on the overall mechanical properties of these films. This method may be applicable to a variety of thin transparent films. The 2α peak can be observed in both supported and free-standing films;[24,25] in the case of supported films, the substrate acts as a reflective surface, whereas for free-standing films, the change in refractive indices between the sample and air causes total internal reflection beyond a specific angle α.

Results and Discussion

PDDA and chitosan polyanions were selected because prior work[1,10] showed fast film growth and high particle loading capacity. To monitor the growth of the films and to determine the elastic constants of the LBL films as a function of thickness, the film thickness was measured every five bilayers (BL), up to 1 μm as shown in Figure 3A. Linear trends are observed for both chit/cellN and PDDA/cellN films with average growth rates of 14 and 19 nm/BL, respectively. For these films the surface roughness increases with thickness, which compromises the accuracy of ellipsometry measurements. Hence, for films thicker than 1 μm we determined their thickness by extrapolating the data in Figure 3A according to the number of bilayers deposited. It should also be noted that the diameter of cellN is roughly 5 nm while a typical polymer chain lying flat on a surface would occupy a space perpendicular to that surface measuring between 1 and 2 nm. Hence, assuming monolayers of polymer and cellN, the minimum thickness of a bilayer would be 6−7 nm, leaving 8−13 nm of unaccounted growth per bilayer. We attribute this extra growth predominantly to the agglomeration of cellNs, as will be discussed later.

Film growth was also monitored using QCM. Figure 3B shows the change in resonant frequency of the quartz crystal after each deposition step for PDDA/cellN, PDDA/cellN/PDDA/PSS, and PDDA/PSS films. The closed symbols indicate the change in frequency after polymer deposition, and the open symbols indicate the change in frequency after cellulose deposition. According to the Sauerbrey equation (eq 4), a larger change in the frequency of the crystal corresponds to a larger change in mass. Figure 3B illustrates that, compared to the polymer layers, the cellN layers contribute significantly more to the increase in mass. Therefore, increasing the relative number of cellN layers, or volume fraction of cellN, should result in an increase in film density, and this has indeed been found as shown in Table 1.

Figures 4 show the elastic constants of chit/cellN and PDDA/cellN composites, containing 73.8 and 84 vol % cellN, respectively, as a function of film thickness between 0.5 and 3 μm. $c_{\parallel,\perp}$ represent the longitudinal elastic constants as defined in Figure 1. Our measurements reveal significant anisotropy between the elastic responses of LBL films in plane and in growth direction. To verify whether this anisotropy is the result of the LBL structure or whether it is inherent to the polymer itself, we cast pure PDDA and chitosan films of ~30 μm thickness and measured their elastic constants. For comparison, the corresponding data points are juxtaposed in Figure 4 to those that characterize the various LBL films.

We find that the elastic constant ratios, $c_\parallel/c_\perp$, for cast PDDA and chitosan films are ~1, suggesting that the cast films of pure polymer are indeed elastically isotropic. If there was any unidirectional setting and drying of cast films, it did not result in any significant elastic anisotropy. In comparison, for LBL films containing cellN the stiffness in the growth plane is approximately a factor of 2 larger than in the growth direction for both the chitosan and PDDA system. Within the layers stiffness is enhanced due to the spatial overlap between the high-modulus embedded fibers in the direction of strain, i.e., any arbitrary cross section perpendicular to this direction will intersect fibers, while

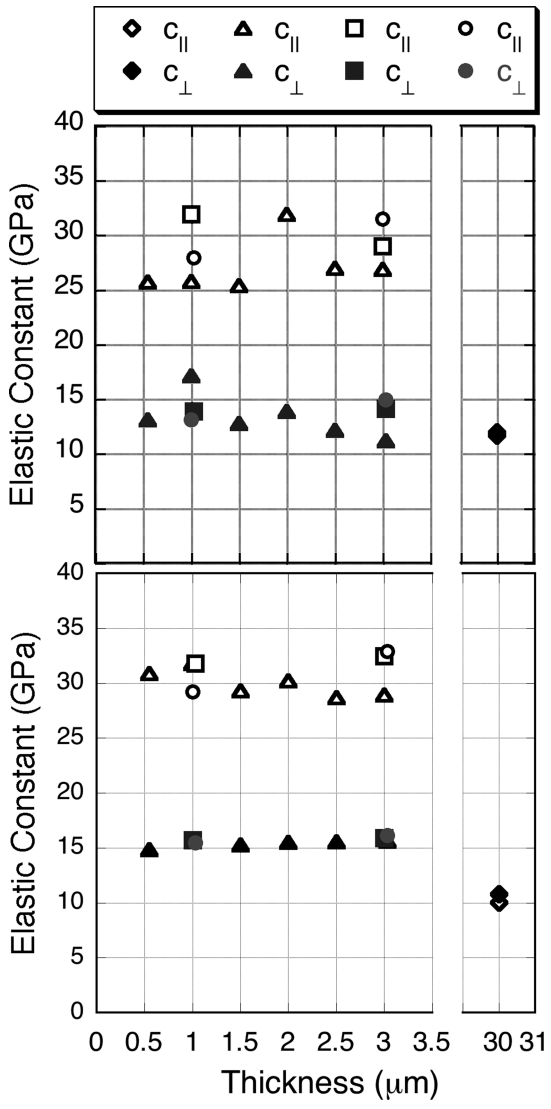

Figure 4. Elastic constants of (A) chit/cellN and (B) PDDA/cellN films as a function of thickness for as-is and heat-treated films: ◆, cast polymer film; ▲, polymer/cellN set A; ■, polymer/cellN set B; ●, polymer/cellN set B after heat treatment.

the polymer in adjacent layers serves to transmit load between fibers, both laterally and end-to-end. In general terms, we should therefore expect the in-plane modulus to be that of elastic components acting in parallel, i.e., an appropriately weighted average of the polymer and fibers moduli. Conversely, in the growth direction, the fibers do not stretch across all layers, and their load-bearing ability is distinctly interrupted by the polymer layers. In this direction we would expect the elastic response of the film to be dominated by the most compliant constituent, as expected for components with different stiffness configured in series, where the reciprocals of the moduli of polymer and fibers, prorated according to their relative effective proportions, are additive. A detailed numerical model describing the elastic behavior of our LBL films is derived below.

However, first we note that here are significant differences in the extents to which these anisotropies are manifest in LBL films, depending whether they involve PDDA or chitosan polymer layers. The elastic constants in the growth planes ($c_{||}$) are about 2 and 3 times that of the corresponding cast films for chit/cellN and PDDA/cellN, respectively. The average $c_{\perp}$ for PDDA/cellN films is about 50% higher than that of cast PDDA film, whereas the average $c_{\perp}$ for chit/cellN films is roughly the same as for the cast

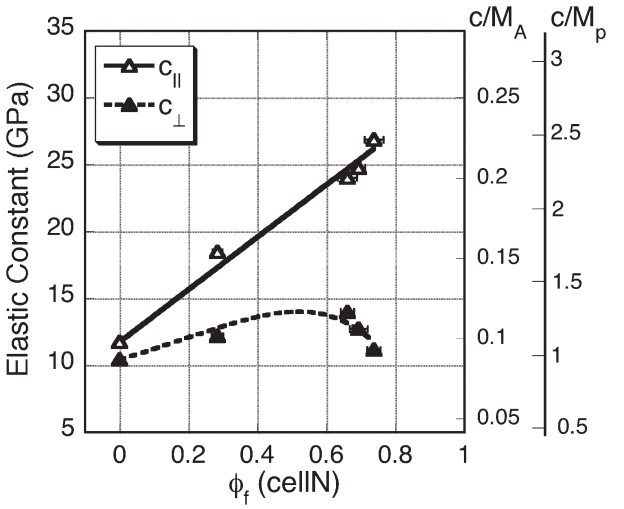

Figure 5. Elastic constants of $[(\text{chit/cellN})_x/(\text{chit/PSS})_y]$ films as a function of cellN volume fraction.

chitosan film. Addition of cellN fibers therefore has a significantly more dramatic effect on both the in-plane and out-of-plane elastic properties of PDDA/cellN LBL films than those of chit/cellN films. Presumably, this is the result of the differences in adhesion between fiber and polymer facilitating a better fiber-to-matrix load transfer in the case of PDDA/cellN composites, either through larger contact areas or stronger bonding. This interpretation of the elastic modulus data is consistent with observations made from mass adsorption using the QCM. The average change in resonance frequency per added polymer layer is ~5.2 Hz for chit/cellN, while it is ~11.2 Hz for PDDA/cellN, indicating that more than twice the amount of PDDA adheres to the cellN (surface of the film) per deposition step. Similarly, the average per-layer change in resonance frequency for cellN is ~116 and 162 Hz for chit/cellN and PDDA/cellN, respectively. Other processing parameters, such as cellN solution used, film thickness, and heat treatment, do not have a significant effect on the stiffness for either film. The invariance of the modulus as a function of film thickness is in agreement with previous findings of isotropic and layered thin films using BLS.[19,22]

Several factors can contribute to the contrasting elastic responses of nanocomposites in which otherwise identical fibers are sandwiched between PDDA or chitosan layers. These include differences in wetting or bonding behavior between fiber and polymer, the formation of different in interfacial structures, or dissimilar permeation of the solution into previously deposited layers upon dip coating, possibly resulting in different fiber orientation. To gain further insight and possible explanations for the observed behaviors, we measured the elastic constants as a function of cellN volume fraction and analyzed the results in terms of simple mechanical models. Layers of PSS were incorporated to create $[(\text{polymer/cellN})_x/(\text{polymer/PSS})_y]$ structures (sometimes referred to as polymer/cellN/PSS films) with variable number of cellN layers, while the total thickness of the films was held constant at 1 μm; in other words, the individual polymer layer thickness varies while the cellN layer thickness remains the same. Figures 5 and 6 show the in-plane and out-of-plane elastic constants of $[(\text{polymer/cellN})_x/(\text{polymer/PSS})_y]$ as a function of cellN volume fraction, ϕ_f, where "polymer" refers to either chitosan or PDDA. Therefore, for $\phi_f = 0$, the LBL film is a polymeric film of either PDDA/PSS or chit/PSS bilayers without any fibers added, and at $\phi_f = 1$ the system contains no polymer; the fibers held together solely by van der Waals forces or chemical bonding in case fibers were not fully separated during hydrolysis. $c_{||}$ increases fairly linearly with increasing amount of cellN; this

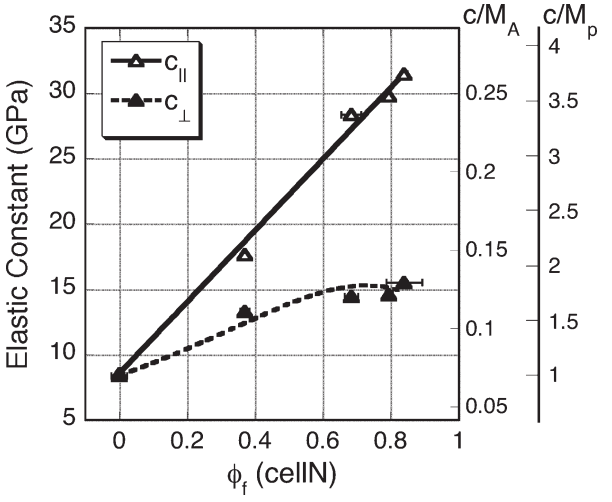

Figure 6. Elastic constants of $[(PDDA/cellN)_x/(PDDA/PSS)_y]$ films as a function of cellN volume fraction.

effect was observed previously for mixed cellulose or cellN reinforced polymer composites, where the in-plane modulus grew from 1.5 to 20 GPa with increasing amount of cellulose.[26−30] $c_\perp$ increases with increasing amounts of cellN as well for both systems, but at a rate that is slower than that of $c_\parallel$. Accordingly, the addition of cellN always provides an initial increase in stiffness in the growth direction. However, the beneficial effect on the composite stiffness due to increasing the amount of cellN eventually subsides for lack of sufficient bonding agent linking the fibers. This can be observed particularly in the case of chit/cellN/PSS films where the out-of-plane elastic constant ($c_\perp$) reaches a maximum and starts to tail off at around 60% fiber volume concentration. By contrast, a decrease in $c_\perp$ for PDDA/cellN films is not observed within the achievable range of fiber loadings. This supports our earlier claim that a better fiber-to-matrix load transfer occurs in the PDDA/cellN films because a higher density of contact points is achieved in the thicker individual PDDA layers.

In order to interpret our data in terms of the structural definition of the interfaces in these multilayer films, specifically the degree of intermixing of polymer and cellN layers, we explored various approaches for modeling the observed elastic characteristics. The model that best describes our findings is derived in the following. As stated above, the initial premise for this model was that the in-plane modulus could be closely described by elastic elements in parallel, whereas the out-of-plane modulus would more likely involve elastic elements in series. We then refined the corresponding expression to account for deviations from these simplified assumptions based on our perception of the structural developments that take place during LBL deposition. Hence, we begin with the expressions

$$c_\parallel = \phi_f M_f^\parallel + (1-\phi_f) M_p^\parallel \tag{8}$$

and

$$c_\perp = \left(\frac{\phi_f}{M_f^\perp} + \frac{1-\phi_f}{M_p^\perp} \right)^{-1} \tag{9}$$

where $M_f^\parallel$ and $M_p^\parallel$ are the effective longitudinal elastic moduli of the fiber and the polymer layers, respectively, as they contribute to the in-plane composite modulus, while $M_f^\perp$ and $M_p^\perp$ are the effective moduli of the two layers as they contribute to the out-of-plane composite modulus. Note that by assuming the polymer volume fraction to be $\phi_p = 1 - \phi_f$, we ignore the porosity of the film in the material balance. However, the effect of porosity is implicitly accounted for upon evaluating the magnitudes of the fiber and polymer layer moduli.

Because of its amorphous structure, the properties of the polymer phase are isotropic and the elastic modulus is independent of direction; thus, $M_p^\parallel \cong M_p^\perp = M_p$. On the other hand, the elastic properties of a single cellN are anisotropic; the axial modulus of the fiber is much higher than the radial one.[6] During LBL deposition, fibers are deposited so that their length axes orient randomly within the space defined by the two in-plane dimensions.[1] Even though that would still provide for an isotropic modulus within the plane, its magnitude deviates from the axial modulus of the fiber. There are a number of models, most notably the Voigt−Reuss,[31,32] Halpin−Tsai,[33] and Cox models,[34] that describe the stiffness of randomly oriented short fibers embedded in a continuous matrix as a function of the fiber concentration. Cox's shear-lag concept provides a correction η_L to the effective modulus of a composite to account for the incomplete load transmission between fiber and matrix, as these strain by different amounts due to their different moduli, i.e.

$$\eta_L = 1 - \frac{\tanh(\beta l/2)}{\beta l/2} \tag{10}$$

where

$$\beta = \left[\frac{2G_p}{R^2 M_A \ln(r/R)} \right]^{1/2}$$

Here l and R are the length and radius of the fiber, respectively, r is the interfiber spacing, G_p is the shear modulus of the polymer matrix, and M_A is the axial modulus of the fiber, i.e., $M_A = 120$ GPa.[5,6] Krenchel[35] built onto Cox's model and corrected for the effect of nonuniform fiber orientation by introducing the factor

$$\eta_0 = \sum_n a_n \cos^4 \theta_n \tag{11}$$

where a_n is the ratio of fiber with an orientation of angle θ_n. For a 2D system of randomly oriented in-plane fibers with lengths of 300 nm, η_L and η_0 are 0.932 and 0.375, respectively. Unlike traditional composites, however, in our LBL films cellN fibers are only partially embedded in the polymer of the adjacent layers. Within the fiber layer there may be regions of overlapping fibers and incomplete polymer penetration. The stiffness reduction due to this porosity is accounted for by introducing the factor η_p. The expression for the in-plane modulus then adjusts to

$$c_\parallel = \phi_f \eta_p \eta_0 \eta_L M_A + (1-\phi_f) M_p \tag{12}$$

While this expression for the in-plane stiffness is entirely compatible with the traditional rules-of-mixture for elastic elements in parallel, i.e., it describes a linear dependence of elastic constant on the volume fraction of fibers, the observed out-of-plane stiffness deviates from what a combination of elastic elements in series would predict, especially for chit/cellN where the modulus decreases at high fiber loading. We attribute this to the fact that the individual layers deposited during the LBL process do not form a sharply defined interface with each other but that there are high levels of interpenetration of fibers into the polymer layer and polymer into the fiber layer. To account for this mixing of elastic properties, we model the effective moduli for each type of layer in the out-of-plane direction as an appropriately weighted set of elastic elements in parallel, an illustration of the mixed elastic properties can be seen in Figure 7. The polymer that infiltrates the fiber layer is assumed to enhance the load transmission between

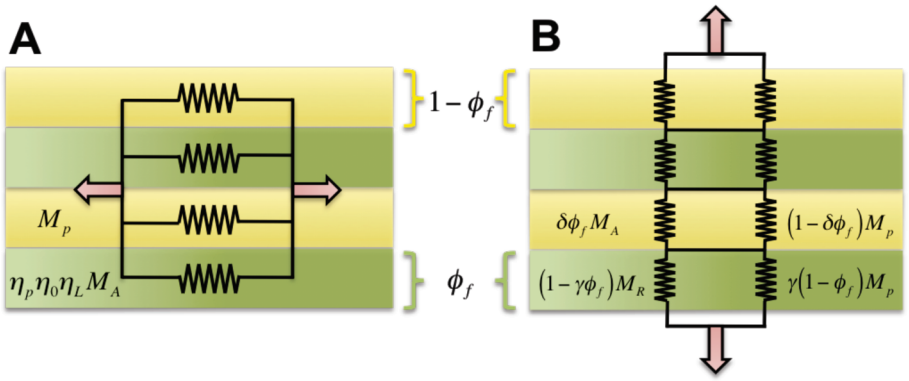

Figure 7. (A) Springs in parallel for elastic constant in the growth plane and (B) springs in series with mixed springs in parallel (as a function of volume fraction) for elastic constant in the growth direction where the yellow and green are the volume fractions of the polymer and fiber, respectively.

Table 2. Best Fit Parameters for the Model Describing the Elastic Constants of Chit/CellN and PDDA/CellN Composites as a Function of CellN Content

	η_p	γ	δ
chit/cellN	0.24	0.914	9.85×10^{-4}
PDDA/cellN	0.28	0.594	0.023

cellN fibers to an extent that is proportional to the overall polymer volume fraction, i.e., the polymer contributes a factor $\gamma(1 - \phi_f)$ of its modulus to $M_f^{\perp}$, so that

$$M_f^{\perp} = (1-\gamma\phi_f)M_R + \gamma(1-\phi_f)M_p \quad (13)$$

where M_R is the stiffness of cellN in the radial direction (30 GPa). As ϕ_f approaches unity, i.e., little or no polymer is available to transmit load between fibers, weak dispersive interactions between fibers take over. This is reflected by the factor $(1 - \gamma\phi_f)$. Similarly, the polymer layers benefit from the stiffness of the fibers to an extent that is proportional to overall volume fraction of fibers, i.e., $\delta\phi_f$. As ϕ_f approaches zero, the contribution from fibers to the stiffness vanishes while that from polymer increases as $(1 - \delta\phi_f)$. Consequently

$$M_p^{\perp} = \delta\phi_f M_A + (1-\delta\phi_f)M_p \quad (14)$$

The expression for the out-of-plane elastic modulus can then be written as

$$c_{\perp} = \left(\frac{\phi_f}{(1-\gamma\phi_f)M_R + \gamma(1-\phi_f)M_P} + \frac{1-\phi_f}{\delta\phi_f M_A + (1-\delta\phi_f)M_P}\right)^{-1} \quad (15)$$

The curves representing the best fits of eqs 12 and 15 to the measured data are shown in Figures 5 and 6 for chit/cellN and PDDA/cellN films, respectively. Table 2 gives a list of the fitting parameters η_p, γ, and δ. In general, γ assumes larger values than δ, which we interpret to mean that the polymer enhances the stiffness of the fiber layer more significantly than fibers affect that of the polymer layer. This makes sense in that we expect the fiber layer to have some porosity, allowing for the polymer to infiltrate the fibers. γ is larger for chit/cellN/PSS than for PDDA/cellN/PSS films, suggesting that it is easier for chitosan to penetrate the fiber layer than for PDDA. This is also supported by the QCM data, according to which the average deposition rate for a cellN layer is lower for that of chit/cellN films, indicating a more porous cellN layer and thus allowing for more polymer penetration. The situation is, however, reversed as far as the magnitude of δ is concerned. Accordingly, during deposition the fibers become more deeply embedded in PDDA than in chitosan, and in fact, the fiber axes deviate more strongly from the in-plane orientation in the PDDA composite. We can therefore expect that the interface between fibers and polymer for PDDA is more diffuse and intermixed and overall forms a mechanically stronger connection than for chitosan. This would also explain why at high fiber loadings the out-of-plane modulus in the PDDA system is larger than that of pure PDDA, while this is not the case for the chitosan system. The small values of δ for both systems suggests that eq 13 in combination with $M_p^{\perp} \simeq M_p$ may be sufficient to describe the data for $c_{\perp}$. However, eq 14 was introduced to account for the possibility that, depending on the sequence of layer depositions, polymer infiltrating the fiber layer may result in a different structure than fibers immersing into the polymer layer. This asymmetry is preserved by eq 14, which indeed provides a better fit to the data for the PDDA/cellN system, especially at low fiber volume fractions.

Conclusion

BLS was used to determine the in-plane and out-of-plane elastic constants of LBL films with different thicknesses and cellN concentrations in backscattering geometry. It was found that the incorporation of cellN increases the stiffness of polymer films more significantly in the in-plane direction as compared to the out-of-plane direction, resulting in elastic anisotropy. Interestingly, for the highest fiber loadings, the out-of-plane moduli for PDDA/cellN films show an improvement from cast PDDA while the out-of-plane moduli for chit/cellN films were similar to those of the cast chitosan film. This suggests a better adhesion and therefore better load transfer between PDDA and cellN. This is the case independent of the cellN contents of the composites. The difference between the elastic responses of chitosan and PDDA based composites is attributed to the quality and definition of the interface between fiber and polymer layers. In the case of the PDDA system this interface is believed to be more diffuse and fibers deviate more from in-plane orientations, so as to stretch across the interface and embed in the polymer layer. In case of the chitosan system the interface is believed to be better defined and more planar, while some polymer separately infiltrates the fiber layer during deposition.

Acknowledgment. The authors thank Prof. Joerg Lahann for the use of their elliposmeter. This project is supported by AFOSR Grant FA9550-05-1-0143.

References and Notes

(1) Podsiadlo, P.; Choi, S. Y.; Shim, B.; Lee, J.; Cuddihy, M.; Kotov, N. A. *Biomacromolecules* **2005**, *6*, 2914–2918.
(2) Podsiadlo, P.; Sui, L.; Elkasabi, Y.; Burgardt, P.; Lee, J.; Miryala, A.; Kusumaatmaja, W.; Carman, M. R.; Shtein, M.; Kieffer, J.; Lahann, J.; Kotov, N. A. *Langmuir* **2007**, *23*, 7901–7906.

(3) Sugiyama, J.; Chanzy, H.; Maret, G. *Macromolecules* **1992**, *25*, 4232–4234.
(4) Samir, M. A. S. A.; Alloin, F.; Dufresne, A. *Biomacromolecules* **2005**, *6*, 612–626.
(5) Ishikawa, A.; Okano, T.; Sugiyama, J. *Polymer* **1997**, *38*, 463–468.
(6) Tashiro, K.; Kobayashi, M. *Polymer* **1991**, *32*, 1516–1530.
(7) Bledzki, A. K.; Gassan, J. *Prog. Polym. Sci.* **1999**, *24*, 221–274.
(8) Gandini, A. *Macromolecules* **2008**, *41*, 9491–9504.
(9) Zadorecki, P.; Michell, A. *Polym. Compos.* **1989**, *10*, 69–77.
(10) Bertrand, P.; Jonas, A.; Laschewsky, A.; Legras, R. *Macromol. Rapid Commun.* **2000**, *21*, 319–348.
(11) Decher, G. *Science* **1997**, *277*, 1232–1237.
(12) Hammond, P. T. *Adv. Mater.* **2004**, *16*, 1271–1293.
(13) Lutkenhaus, J. L.; McEnnis, K.; Hammond, P. T. *Macromolecules* **2008**, *41*, 6047–6054.
(14) Wosnick, J. H.; Liao, J. H.; Swager, T. M. *Macromolecules* **2005**, *38*, 9287–9290.
(15) Sperling, L. H. *Introduction to Physcial Polymer Science*; John Wiley & Sons, Inc.: Hoboken, NJ, 2006.
(16) Fengel, D. *Holz Roh- Werkst.* **1984**, *42*, 276–276.
(17) Sauerbrey, G. *Z. Phys.* **1959**, *155*, 206–222.
(18) Cheng, W.; Sainidou, R.; Burgardt, P.; Stefanou, N.; Kiyanova, A.; Efremov, M.; Fytas, G.; Nealey, P. F. *Macromolecules* **2007**, *40*, 7283–7290.
(19) Gomopoulos, N.; Cheng, W.; Efremov, M.; Nealey, P. F.; Fytas, G. *Macromolecules* **2009**, *42*, 7164–7167.
(20) Brillouin, L. *Ann. Phys.* **1922**, *17*.
(21) Carlotti, G.; Fioretto, D.; Socino, G.; Verona, E. *J. Phys.: Condens. Matter* **1995**, *7*, 9147–9153.
(22) Gomopoulos, N.; Saini, G.; Efremov, M.; Nealey, P. F.; Nelson, K.; Fytas, G. *Macromolecules* **2010**, *43*, 1551–1555.
(23) Hillebrands, B.; Lee, S.; Stegeman, G.; Cheng, H.; Potts, J. E.; Nizzoli, F. *Phys. Rev. Lett.* **1988**, *60*, 832–835.
(24) Rioboo, R. J. J.; Souto, J.; de Saja, J. A.; Prieto, C. *Langmuir* **1998**, *14*, 6625–6627.
(25) Nizzoli, F.; Hillebrands, B.; Lee, S.; Stegeman, G.; Duda, G.; Wegner, G.; Knoll, W. *Phys. Rev. B* **1989**, *40*, 3323–3328.
(26) Bataille, P.; Ricard, L.; Sapieha, S. *Polym. Compos.* **1989**, *10*, 103–108.
(27) Noishiki, Y.; Nishiyama, Y.; Wada, M.; Kuga, S.; Magoshi, J. *J. Appl. Polym. Sci.* **2002**, *86*, 3425–3429.
(28) Nishino, T.; Matsuda, I.; Hirao, K. *Macromolecules* **2004**, *37*, 7683–7687.
(29) Uesaka, T.; Nakane, K.; Maeda, S.; Ogihara, T.; Ogata, N. *Polymer* **2000**, *41*, 8449–8454.
(30) Yamanaka, S.; Watanabe, K.; Kitamura, N.; Iguchi, M.; Mitsuhashi, S.; Nishi, Y.; Uryu, M. *J. Mater. Sci.* **1989**, *24*, 3141–3145.
(31) Reuss, A. *Z Angew Math. Mech.* **1929**, *9*, 49–58.
(32) Voigt, W. *Ann. Phys.* **1889**, *38*.
(33) Matthews, F. L.; Rawlings, R. D. *Composite Materials: Engineering and Science*; Woodhead Publishing Limited: Abington Hall, 1999.
(34) Cox, H. L. *Br. J. Appl. Phys.* **1952**, *3*, 72–79.
(35) Krenchel. *Fibre Reinforcement*; Akademisk Forlag: Copenhagen, 1964.